

Unlocking Metasurface Practicality for B5G Networks: AI-assisted RIS Planning

As accepted in the IEEE Global Communications Conference 2023

Guillermo Encinas-Lago^{*†}, Antonio Albanese^{‡§}, Vincenzo Sciancalepore^{*},
Marco Di Renzo[†], Xavier Costa-Pérez^{*¶}

^{*}NEC Laboratories Europe, 69115 Heidelberg, Germany

[†]Université Paris-Saclay, CNRS, CentraleSupélec, Laboratoire des Signaux et Systèmes, 91190 Gif-sur-Yvette, France

[‡]Departamento de Ingeniería Telemática, University Carlos III of Madrid, 28911 Leganés, Spain

[§]Flyhound Co., 10019 New York, US

[¶]i2cat Foundation and ICREA, 08034 Barcelona, Spain

Abstract—The advent of reconfigurable intelligent surfaces (RISs) brings along significant improvements for wireless technology on the verge of beyond-fifth-generation networks (B5G). The proven flexibility in influencing the propagation environment opens up the possibility of programmatically altering the wireless channel to the advantage of network designers, enabling the exploitation of higher-frequency bands for superior throughput overcoming the challenging electromagnetic (EM) propagation properties at these frequency bands.

However, RISs are not magic bullets. Their employment comes with significant complexity, requiring ad-hoc deployments and management operations to come to fruition. In this paper, we tackle the open problem of bringing RISs to the field, focusing on areas with little or no coverage. In fact, we present a first-of-its-kind deep reinforcement learning (DRL) solution, dubbed as D-RISA, which trains a DRL agent and, in turn, obtains an optimal RIS deployment. We validate our framework in the indoor scenario of the Rennes railway station in France, assessing the performance of our algorithm against state-of-the-art (SOA) approaches. Our benchmarks showcase better coverage, i.e., 10-dB increase in minimum signal-to-noise ratio (SNR), at lower computational time (up to -25%) while improving scalability towards denser network deployments.

I. INTRODUCTION

Current social and industrial trends call for superior all-around network capabilities. Phenomena like the proliferation of smart devices or large-scale Internet of Things (IoT) deployments require wider bandwidths, coverage ubiquity, improved localization accuracy, and network deployments able to serve much more densely populated areas. This impelling need is directly shaping future technology standards, pushing the boundaries of network operators, which continuously investigate disruptive solutions to enable never-decreasing revenue streams while satisfying the customers' growing demand for network performance [1].

Although the adoption of millimeter-wave (mm-Wave) frequencies is a key enabler of such use cases for fifth-generation (5G) and beyond-fifth-generation networks (B5G) networks,

those frequencies present higher attenuation and poor propagation properties, requiring direct line-of-sight (LoS) paths between base stations (BSs) and user equipments (UEs) to compensate for such relevant power losses. Reconfigurable intelligent surfaces (RISs) pave the way to substantial beam-forming gains packing a massive number of configurable passive reflectors (e.g., built using varactor diodes) equipped with low-cost and low-complexity electronics [2].

The key value of RISs—adaptive reconfigurability—allows focusing the impinging signals onto some desired directions and dynamically altering the reflection at will, while drawing minimal power, installation and maintenance costs compared to deploying active BSs. This makes RISs an effective candidate technology to tackle the mobile dead-zone problem in challenged scenarios, e.g., in classical indoor environments, at low capital expenditure (CAPEX), by *simply* steering electromagnetic (EM) waves impinging on RISs towards sectors with little to no coverage, dramatically improving the signal-to-interference-plus-noise ratio (SINR) experienced by UEs in those areas [3].

However, RIS deployments still exhibit some practicality issues. As RISs properly funnel the EM energy impinging on their surface carrying useful signal, they might also divert unwanted interference [4], reducing the SINR gains when such effect is not accounted for. Furthermore, current RIS technology—with few notable exceptions employing self-configuring RISs [5]—hinges on an ad-hoc control channel to distribute the optimal reflection configurations to multiple RISs managed by a common centralized controller.

It is therefore crucial to contain the extension of such channel, which would increase complexity and deployment costs, thus limiting the agility of RIS-enabled networks. In this regard, advanced optimization techniques need to be developed and employed at the network planning stage, aiming at identifying the optimal trade-off among network coverage, interference reduction, and RISs density [6], [7]. In order to

retain the low CAPEX benefits of these devices, the newly developed methods (as our deployment solution) for RISs need to be also computationally inexpensive.

A. Contributions

In this paper, we propose D-RISA, namely Deep RIS-Aware network deployment and planning, as a novel deep reinforcement learning (DRL)-based solution to enable practical installations of RISs in the field by raising a *digital twin* of the environment performed via a ray tracing simulation and a 3D model of the target area.

We introduce a paradigm shift in the use of DRL to solve RIS deployment problems by not aiming at producing a DRL agent able to solve any problem instance, but rather tailoring the training of D-RISA to the specific problem at hand, making it less demanding with respect to the available literature while avoiding the discretization of the solution space and thus increasing the solution scalability.

In particular, the contributions made by this paper can be summarized as follows: we *i*) translate the RIS deployment problem into a DRL problem by means of the bespoke space and action spaces design, *ii*) identify the minimum signal-to-noise ratio (SNR) as a feasible metric to be computed by a custom-made ray tracing simulator to feed the DRL training process, *iii*) make use of the D-RISA DRL agent training phase as an exploration tool to find the best deployment solution, avoiding the need for a complete viable agent, *iv*) showcase the rapid convergence of the agent solution and *v*) benchmark D-RISA against the state-of-the-art (SOA) as well as exhaustive approaches, demonstrating outstanding performance while emulating the indoor scenario of a real environment, namely the Rennes railway station in France.

TABLE I: List of abbreviations

5G	fifth-generation	BSG	beyond-fifth-generation networks
AI	artificial intelligence	CAPEX	capital expenditure
AoD	angle of departure	CSI	channel state information
BS	base station	DQfD	deep Q-learning from demonstrations
CS	candidate site	DRL	deep reinforcement learning
DQL	deep Q-learning	ITU	International Telecommunication Union
EM	electromagnetic	MIMO	multiple-input and multiple-output
ES	exhaustive search	MLP	multilayered perceptron
FP	fractional programming	MRT	maximum ratio transmission
IoT	internet of things	ReLU	rectified linear unit
LoS	line-of-sight	RIS	reconfigurable intelligent surface
mm-Wave	millimeter-wave	SBR	shooting and bouncing rays
NLoS	non-line-of-sight	SINR	signal-to-interference-plus-noise ratio
PLA	planar linear array	SNCF	Société nationale des chemins de fer français
SNR	signal-to-noise ratio	TDMA	time-division multiple access
SOA	state-of-the-art	UAV	unmanned aerial vehicle
TP	test point	UCA	uniform circular array
UE	user equipment	URA	uniform rectangular array
ULA	uniform linear array		

II. FRAMEWORK OVERVIEW

Hereafter, we tackle the problem of efficiently deploying RISs in a known environment. We extend a currently existing network deployment with RISs to eliminate coverage dead zones. We consider the environment of the Rennes railway station hall, operated by the French Société nationale des chemins de fer français (SNCF)¹, and visualized in Fig. 1. In

¹We build the 3D model from the architectural data, and the information provided by the network operator servicing the area.

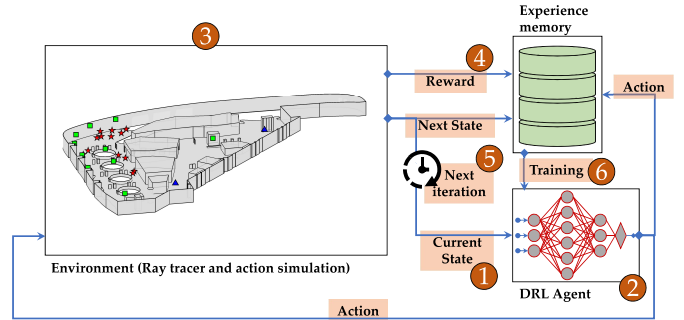


Fig. 1: D-RISA’s building blocks showing the training process for a given frame. In the 3D map, the candidate sites (CSs) for the RIS deployment are shown in green, the BSs in blue, and test points (TPs) in red.

the present work, we try to alleviate the dead zone problem. The current deployment of BSs in the Rennes station has several areas with connectivity problems due to the low SNR achieved. We identify and set TPs on those locations and alleviate the problem with our proposed solution. Specifically, we make use of a custom-made ray tracing engine to simulate any proposed deployment in the scenario while accounting for its current network infrastructure, provided by a major European network operator. As the ray tracer outputs the values of the objective function (the minimum SNR across all the TPs defined, as described in Section III) we train a DRL solution by using them as rewards.

In Fig. 1, we showcase the main building blocks of our proposed solution, itemizing the operations required for a single training cycle iteration, which is later detailed in Section IV. Here we only assess the main components of D-RISA, namely *i*) a 3D model of the scenario, *ii*) a ray tracer running on such a scenario and capable of evaluating candidate deployment solutions, *iii*) a model for the RIS gain, which we use in combination with the ray tracer to numerically evaluate any solution, *iv*) a Deep Q-Learning (DQL) agent, which takes as input a given solution and decides the best among the different potential changes on it, with the long-term goal of improving the considered objective, and *v*) the training process of the mentioned agent, according to the principles of Deep Q-learning from Demonstrations (DQfD) [8]. We would like to underline that DQL is only one flavor of DRL and that D-RISA can be readily extended to other DRL techniques with minimal modifications.

3D model. The first component of the digital twin—the 3D model of our target scenario—is based on the architectural plans of the Rennes railway station, which is currently equipped with 2 deployed BSs. Similarly to any deployment situation, network operators must comply with regulatory and physical restrictions, thus we consider a predefined number of CSs at which RISs might be deployed². In this work, we handpick the set of CSs, making sure that the installation of RISs at those locations is materially feasible, and ensuring LoS

²We would like to underline that there is no intrinsic limitation on the CSs set, so in principle they could cover the entire target area.

between CSs and both existing BSs and TPs. For the selection of TPs, we focus on the areas experiencing the worst coverage problems under the current BSs-only network deployment. These TPs serve as probe points for the objective and represent UEs to be served after deployment, matching their expected distribution³ [9].

Ray tracer. The second component of the digital twin—the ray tracing simulator—relies on a commercial shooting and bouncing rays (SBR) engine to evaluate any given deployment within a 3D model [10]. To this aim, it computes the possible paths, both LoS and non-line-of-sight (NLoS), between any RIS and any TP or BS. Then, it derives their geometric information (i.e., the angle of departure (AoD) from the RIS), which is fundamental for assessing the end-to-end path losses and so the objective function for the given deployment. Thanks to the use of the ray tracer, our approach does not need to make assumptions on the BS-RIS-TP channels, as they are individually simulated: any fading is therefore taken into account in the solution.

RIS gain model. As mentioned in Section I, we face a chicken-egg problem. To decide the best deployment of RISs we need to start from a known configuration, whereas the optimal configurations can be computed only upon fixing the deployment and the BS-RIS-TP associations. Here we anticipate that we overcome the problem by considering a cellular-like architecture in which each RIS serves one contiguous subarea, thus reducing the scope of inter-RIS interference to the edges of said subareas. Then, to achieve full decoupling of the BSs and RISs beamforming optimization from the planning problem, we assume that each BS can be associated to multiple RISs, while operating in a time-division multiple access (TDMA) fashion, namely radiating towards one of them at a time, thereby allowing maximum ratio transmission (MRT) precoding at the BSs. In these conditions, the RIS gain model can be obtained by means of beam broadening and flattening as per [11]. It is worth noting that the approach detailed in [11] assumes continuous phase shifts for the RISs, and hence we inherit that assumption. Nevertheless, this technique, based on the sub-division of the device in sub-RISs that act in coordination, can be applied to discrete phase models for the RISs, with minimal performance losses due to the phase discretization [12]. Additionally, we design D-RISA to be completely decoupled from the RIS model used to compute the SNR, and hence, the gain of the RIS. We further analyze the RIS planning problem in Section III.

DQL agent. In Section IV, we design the DQL agent used to explore the space of possible deployments. Our DQL agent considers deployments and identifies the best actions to improve them (e.g., placing an RIS at a specific CS). Such improvement is not obtained by means of a mere greedy approach. On the contrary, the D-RISA agent attempts to evolve the solution to the one maximizing the objective. By training the agent, we explore possible deployments combining

³Please note that D-RISA does not make any assumption on the specific UEs or TPs distributions.

acquired knowledge and random exploration, and find the best deployment solution upon stopping the training of the agent when the related criteria are met.

III. RIS PLANNING

We consider an RIS-enabled network comprising of L RISs deployed to aid a pre-existing deployment of M BSs in order to reduce the areas with limited or no coverage. Each BS is a uniform linear array (ULA) of N_b antennas, and each RIS is a planar linear array (PLA) of $N_r = N_h \times N_v$ reflective elements, where N_h and N_v denote the number of elements in the horizontal and the vertical directions, respectively. A symbol received at the UE through the cascaded channel BS-RIS-UE is formulated according to the channel and the RIS element configuration, as the following:

$$y = (\mathbf{h}^H \Theta \mathbf{G}) \mathbf{w} s + n \in \mathbb{C}, \quad (1)$$

where \mathbf{h}^H represents the Hermitian transposition of the channel between the RIS and the receiver, $\Theta = \text{diag}(\alpha_1 e^{j\phi_1}, \dots, \alpha_N e^{j\phi_N})$ with ϕ_i and α_i representing the phase shift and magnitude of the i -th element of the RIS, \mathbf{G} is the channel between the elements of the RIS and the individual antennas of the BS, \mathbf{w} is the vector of transmit weights of the BS antennas while s is the transmitted symbol, and n is the additive white Gaussian noise term distributed as $\mathcal{CN}(0, \sigma^2)$. Since we do not specialize any mathematical expressions based on the distribution of the BS elements, the assumption of ULA shape can be generalised to other arrangements, including uniform circular arrays (UCAs), uniform rectangular arrays (URAs), as long as they can be adequately modeled and computed. For our model, we rely on a ray tracer engine, overcoming the need for channel estimation and models. As mentioned in Section II, we configure the RISs to serve their respective subarea using the beam broadening and flattening technique proposed in [11]. We subdivide each RIS in sub-sections so that they interfere constructively to obtain a beam of constant gain and controlled width. The gain of such beam g depends only on the number of elements and shape of the RIS, namely

$$g(N_h, N_v, \Delta_y, \Delta_z) \propto \frac{N_h^2}{\Delta_y N_h \delta} \frac{N_v^2}{\Delta_z N_v \delta}, \quad (2)$$

where δ is the ratio between the RIS inter-element distance and the signal wavelength, and Δ_y and Δ_z are the spatial frequencies comprised in the beam in both directions, as illustrated in Fig. 2. Using this gain and the antenna models of the BSs and UEs, we compute the SNR of the individual TPs under a given deployment.

We can now formulate the objective function as follows

$$\max_{\mathcal{S}} \min_{\mathbf{u}_t} \text{SNR}(\mathbf{u}_t), \quad (3)$$

in which \mathcal{S} denotes the solution space, defined as the set of possible BS-RIS-TP associations and possible RIS deployments, while \mathbf{u}_t represents the coordinates of test point t , with $t = 0, \dots, T - 1$, where T is the number of considered test points. The solution space \mathcal{S} is thoroughly analyzed in

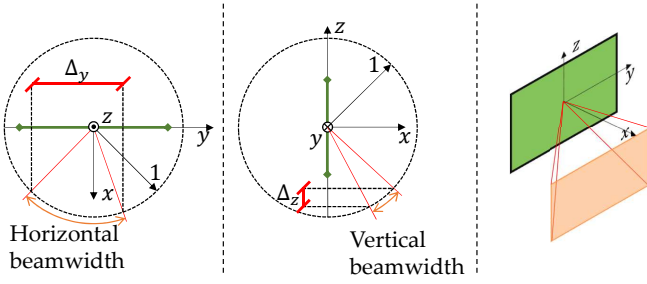


Fig. 2: Geometry of the RIS gain model.

Section IV. By indicating the number of CSs for the RIS deployment as $N \geq L$, the considered problem consists of selecting L out of N CSs to deploy the RISs and identifying the associations with BSs and TPs.

A conventional approach to tackle the problem of optimally deploying RISs is to extend known algorithms used for the deployment of non-multiple-input and multiple-output (MIMO) and MIMO networks. The problem can then be written as an optimization problem and tackled with non-convex optimization tools. It can be relaxed via Fractional Programming (FP) to derive a tractable form, obtaining approximate solutions after binary rounding [13]. However, such methods are model-based, and are not able to consider the actual propagation environment. On the other hand, DRL, being data-driven, can leverage large measurement sets to tailor the deployment to the EM properties of the target area. Ray tracing simulations can generate the training data at the planning stage using 3D models.

Q-learning. D-RISA relies on a model-free DRL technique, DQL. It operates in a space of possible states \mathcal{S} , and a space of actions \mathcal{A} that can be taken in each state. Each action taken evolves the state into a new one, and produces a reward. A quantity Q is associated with each pair state-action, based on immediate and potential future rewards. The policy of the algorithm is to choose, for each state, the action with the highest Q value.

To train a Q-learning agent, we feed it with states from space \mathcal{S} , and allow it to make random choices (*exploration*) or informed choices based on its past learning (*exploitation*). The atomic element of the training process is the frame. A frame considers an initial state $s \in \mathcal{S}$, an action $a \in \mathcal{A}$ chosen by the Q-learning agent or randomly picked, and the state evolution to the next state $s' \in \mathcal{S}$, producing a reward $r(s, s') \in \mathbb{R}$. The balance between exploration and exploitation varies with time, beginning with a preponderance of exploration to end mostly with exploitation. To randomize the individual decisions, if the total number of frames for a training run is predetermined to be F , at a given frame f , an exploratory action happens with probability $P_{explore} = 1 - (f/F)$ and an exploitative action with a probability $P_{exploit} = f/F$. After each training frame, Q-learning updates the associated value $Q(s, a)$ as

$$Q_{new}(s, a) = (1 - \alpha_q) Q_{old}(s, a) + \alpha_q \left[r(s, s') + \gamma_q \max_{a \in \mathcal{A}} Q(s', a) \right], \quad (4)$$

where α_q determines the training speed, γ_q determines how much potential future rewards affect the action selection, and Q_{old} and Q_{new} are the existing and updated values for $Q(s, a)$.

IV. SOLUTION BY SPACE EXPLORATION

We describe here in detail the D-RISA DQL agent. The structure of DQL builds upon the conventional Q-learning by substituting the Q-table with a neural network and adapting the training process. This way, the agent is not restricted to finite or discrete state and action spaces and avoids the large memory requirements of Q-learning. Additionally, the neural network learns from past data and infers patterns, even when encountering situations that have never been experienced before.

Analogously to Q-learning, we perform the training of the agent with a series of frames, grouped into episodes: an episode begins with a random initial state (no. 1 in Fig. 1) and evolves as a consequence of the actions taken (no. 2 in Fig. 1). For each action taken, the environment produces a reward (no. 3 and 5 in Fig. 1). The episode ends when the DQL agent chooses the stop action or when the maximum number of frames is reached, as described in the following. D-RISA follows the same exploration-exploitation strategy as Q-learning.

For each frame we record the initial state, the action taken, the final state and the reward in the experience memory buffer (no. 4 in Fig. 1). With a predetermined frequency T_T , the neural network NN that substitutes the Q-table is retrained using a random selection of those records (no. 6 in Fig. 1). To compute the Q-values necessary to do so, we employ a copy NN' of NN to predict an estimation of the future rewards for each data instance of the selection of records from the buffer, namely

$$\max_{a \in \mathcal{A}} Q(s', a) \approx \max_{a \in \mathcal{A}} NN'(s', a). \quad (5)$$

Hence, we define the reference Q-values for each selected record as

$$Q_{ref}(s, a) \triangleq r(s, s') + \gamma_q \max_{a \in \mathcal{A}} NN'(s', a). \quad (6)$$

We define a loss function to reward the ability of the neural network to mimic the Q_{ref} values derived from the selected records. We compute the gradient of such loss function with respect to the trainable weights of the neural network, and we update the weights in the gradient direction. The neural network NN' is updated by copying NN with a frequency T_{ST}^{-1} , with $T_{ST} \gg T_T$. This way we prevent the instability of the training process, which makes use of the neural network recursively, since retraining the network may affect the estimation of future rewards and, in turn, affect the whole training

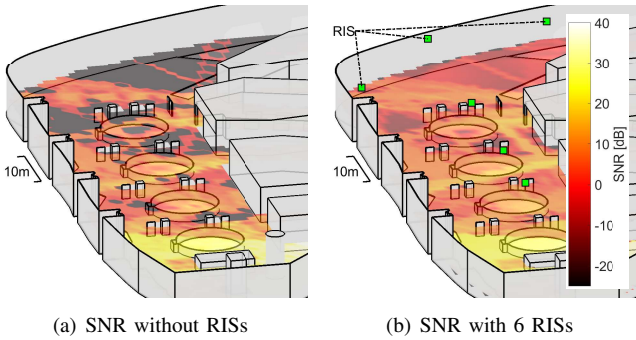


Fig. 3: SNR analysis considering (a) the current arrangement and (b) the SNR achievable with $L = 6$ RISs.

process. Using this method to navigate the state space, the D-RISA agent is able to find viable deployment solutions. For allowing the operation of the agent, we formulate the solution space \mathcal{S} and action space \mathcal{A} as follows.

Solutions space. An individual state (or solution) $s \in \mathcal{S}$ consists of deployment and association. The deployment is formulated as a binary vector $\mathbf{x} = \{0, 1\}^N$, where $x_n = 1$ represents a deployed RIS at CS n . The association is translated into a binary matrix $Y \in \{0, 1\}^{L \times T}$, where $y_{l,t} = 1$ indicates that the deployed RIS l provides coverage to the TP t . Concatenating the binary deployment vector \mathbf{x} with the individual rows of the association matrix Y , we obtain a binary representation of the state that the agent can handle.

Actions space. In D-RISA, we define the following actions: *i*) place a deployed RIS at a chosen CS, *ii*) remove a deployed RIS from a chosen CS, *iii*) change the association of a chosen TP to the next available RIS, *iv*) change the association of a chosen TP to the previous available RIS, *v*) end the current episode.

Alternative deployments. Current SOA RIS prototypes, as the one presented in [14], are expected to have highly affordable mass-producing costs. Other techniques, such as smart skins, can attain similar properties with even simpler implementations, cheaper maintenance, and no electric consumption for operation, at the cost of no reconfigurability [15]. In this work, we assume very limited capabilities for the RIS to be able to reconfigure itself, either due to time or energy constraints. This flexibility allows D-RISA to be applied to passive and static reflection technologies, such as smart skins, as well. The benefits of the capability of RISs to be reconfigurable, in order to meet changing demands and propagation conditions, need to be evaluated in comparison to the traditional option of deploying additional BSs or repeaters, which offers the best performance at the highest cost, or installing RISs for improving the performance while retaining versatility, or even choosing the most affordable smart skin devices but accepting the lack of reconfigurability [15].

V. PERFORMANCE EVALUATION

Simulation settings. We consider the Rennes railway station scenario. D-RISA does not impose a restriction on the

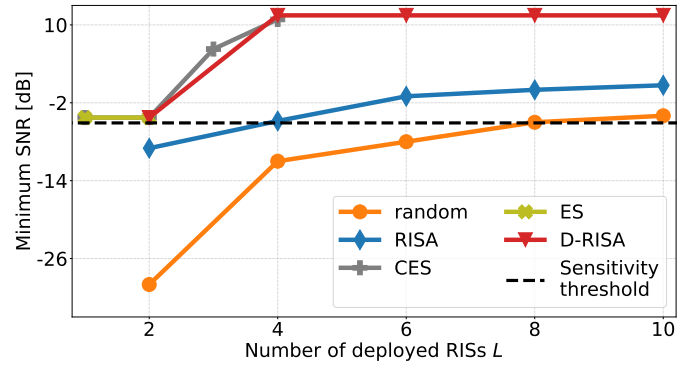


Fig. 4: D-RISA performance against benchmark methods and SOA RISA [13] for a different number of deployed RISs in terms of minimum SNR.

existing infrastructure, and increasing the number of pre-deployed BSs has a negligible impact on the computational costs. Nevertheless, for this work, we reproduce in the ray tracer the currently existing installation of radio equipment in the location by the operator. As a result, we are able to ensure that the actual coverage problems are reproduced in the simulations, and we can obtain practically useful and applicable solutions. The considered scenario is characterized by $M = 2$ existing BSs with a transmit power $P = 28$ dBm operating at $f = 26$ GHz, and select $N = 10$ CSs, and $T = 13$ TPs. The coverage of the area, the positions of the existing BSs and their properties are provided by the European major network operator serving the station. The TPs are scattered in the area, focusing on the sectors wherein existing BSs are not able to provide adequate coverage, while the CSs are handpicked in architecturally suitable places, both in areas directly surrounding the TPs and outside the immediate vicinity, as depicted in Fig. 1. The ray tracer uses a 3D model of the station, which reproduces the most prominent architectural features of the environment. The model is composed of a total of 579 triangular surfaces. It uses the SBR method to find all possible paths between any pair of given points. For simplicity, we use a single material for the whole environment as a reference to compute the losses at each reflection. The material properties are in agreement with the International Telecommunication Union (ITU) values for the permittivity and conductivity of concrete at $f = 26$ GHz, i.e., real part of relative permittivity $Re(\epsilon_r) = 5.31$, and conductivity $\sigma = 0.4557$ S/m [16]. To compute the overall effect of the deployment of RISs in our scenario beyond the chosen test points, we also analyse the whole surface at a height of 1.5 m. To produce such heatmaps, as depicted in Fig. 3 instead of the gain model given in (2), we model the RISs as isotropic scatterers. We can see the difference between the current deployment without RISs in Fig. 3(a) and with RISs in Fig. 3(b).

DQL hyperparameters. We employ a multilayered perceptron (MLP) neural network design with 2 hidden, fully connected layers of 32 neurons activated via a rectified linear unit (ReLU) function. The learning rate and the future

reward reduction are respectively set to $\eta = 0.00025$ and $\gamma_q = 0.99$, which are optimized by means of the Adam algorithm [17]. The training period of the primary network NN is $T_T = 4$ complete frames and the period between updates of the secondary network NN' (i.e., by copying NN) is $T_{ST} = 500$ complete frames. The simulation settings and the DQL parameters are listed in Table II.

TABLE II: Simulation parameters

Parameter	Value	Parameter	Value	Parameter	Value
P	28 dBm	f	26 GHz	N	10
N_h	347	N_v	175	N_b	2
M	2	$Re(\epsilon_r)$	5.31	σ	0.4557 S/m
T	13	γ_q	0.99	T_T	4
η	0.00025	T_T	4	T_{ST}	500

Benchmark. We apply the proposed solution to the described scenario, and put it side-by-side with the following benchmarks: *i*) the solution obtained by exhaustive search (ES), *ii*) the solution obtained by ES considering clusters of TPs instead of individual TPs, drastically reducing the number of possible associations and allowing us to extend the ES up to $L = 4$, *iii*) the solution obtained by means of the SOA RISA [13], which is based on FP, and *iv*) a statistical average of random solutions as previously obtained in the same scenario by [13]. As shown in Fig. 4, D-RISA outperforms all other solutions and matches the ES in terms of minimum SNR at a much lower computational cost. For reference, we also depict the SNR threshold corresponding to the typical receiver sensitivity.

D-RISA training. Fig. 5 illustrates the D-RISA agent training for $L \in \{4, 6, 8\}$ by showcasing the best normalized minimum SNR during each episode and the best solution found at each point in the training process. We observe an increasing trend as the agent keeps building its ability to improve the deployments. As the training process ends with an exploitative behavior (as per Section IV), the high values of the best normalized minimum SNR during each episode suggest that the agent has learned a successful strategy to solve the problem even without exploratory actions.

In some instances, the agent might be unsuccessful in solving the problem at the training end just by leveraging on its own knowledge (exploitation), as depicted in the left side of Fig. 6. Nonetheless, the overall training process is still able to produce a good solution for the RIS deployment problem by combining the exploration and exploitation strategies. Once the training solution convergence is achieved, additional training time would yield a relative minimal improvement w.r.t. the solution: the fully trained agent does not further improve its output by adding more training effort, as shown on the right side of Fig. 6. This implies that the most value of D-RISA is obtained early in the training, thus *allowing for shorter training times and reducing the computational complexity*.

VI. RELATED WORK

The process of deploying cellular networks has been extensively investigated [9], [18], [19], but RIS-enabled network deployment is still an open problem and only a few solutions

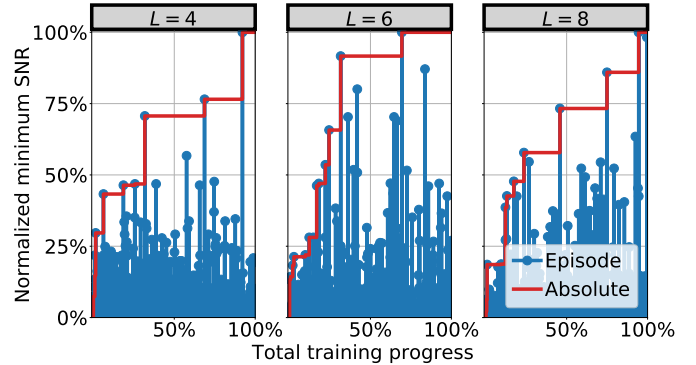


Fig. 5: Solution evolution in terms of normalized minimum SNR for a different number of deployed RISs.

have been proposed. The optimal RIS deployment constitutes a difficult, non-convex problem due to lack of a-priori knowledge on channel state information (CSI) at the planning stage, which generates a *deadlock*: to obtain RIS configurations we need estimations of the BS-RIS-UE channels whereas prior information on RIS configurations is needed to derive the reflection beampattern and so their coverage areas. Even further, optimal RIS configurations might not be able to compensate suboptimal RIS placements: breaking LoS propagation conditions between RISs and BSs or UEs, or resulting in deployments where RISs serve too many UEs that are spread on a wide area, thus reducing the achievable gain [13]. In this context, simplifying assumptions on the geometric CSI can be made, reducing the problem to a more conventional deployment formulation, which can be tackled with techniques akin to well-known BSs deployment approaches [20].

Artificial intelligence (AI) techniques are able to deliver good-quality solutions for highly complex problems and have been proven effective in the context of RISs and, more broadly, MIMO systems, to derive optimal beampatterns [21]–[25]. Likewise, several works in the literature employ DRL approaches to solve the deployment of heterogeneous networks [26] or extremely dynamic scenarios such as unmanned aerial vehicle (UAV)-based networks [27], [28]. As all of the above methods strive to produce fully-fledged DRL agents able to solve any instance of their target deployment problem, they require convergence to the optimal solution to work, which might take an arbitrarily unknown long time and extensive computing resources. This necessity can limit the applicability of the methods whenever the size of the solution (e.g., in terms of deployed devices) grows out of tractability [29], [30].

VII. CONCLUSIONS

The emerging RIS technology shows enormous potential to enable the upcoming generation of wireless networks. However, the solutions to the novel technical problems it poses, such as their intrinsic configuration, design, and deployment, need to be researched to reach a mature SOA. In particular, the deployment problem with its interdependence of the instantaneous RIS configurations unveils unprecedented

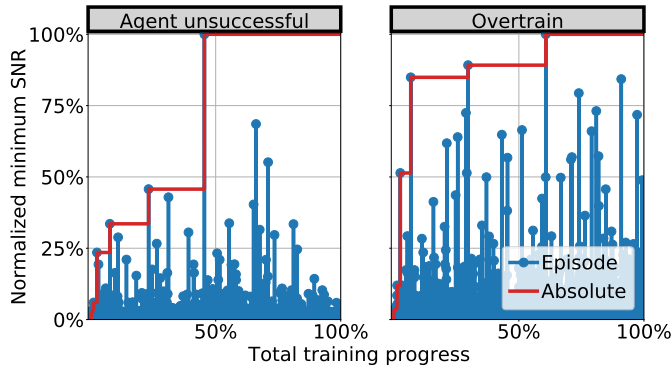


Fig. 6: Solution evolution in terms of normalized minimum SNR for a different number of deployed RISs: (left) unsuccessful D-RISA agent and (right) overtrained (right) D-RISA agent.

challenges that were not involved while considering relays, repeaters, or the deployment of additional BSs.

In this paper, we have proposed D-RISA, a DQL-based, data-driven, model-free solution, which applies the digital twin to train and tackle the optimal deployment issue while taking into consideration the environment and the existing infrastructure. We have benchmarked D-RISA against exhaustive searches and other existing solutions to the problem in a 3D model of the Rennes railway station, outperforming existing solutions by about 10 dB in terms of minimum SNR.

VIII. ACKNOWLEDGEMENTS

This work was supported by EU H2020 RISE-6G (grant agreement 101017011) and EU H2020 METAWIRELESS (grant agreement 956256) projects.

REFERENCES

- [1] W. Saad, M. Bennis, and M. Chen, "A Vision of 6G Wireless Systems: Applications, Trends, Technologies, and Open Research Problems," *IEEE Network*, vol. 34, no. 3, pp. 134–142, 2020.
- [2] E. Björnson, O. Özdogan, and E. G. Larsson, "Reconfigurable Intelligent Surfaces: Three Myths and Two Critical Questions," *IEEE Communications Magazine*, vol. 58, no. 12, pp. 90–96, 2020.
- [3] Y. Liu, X. Liu, X. Mu, T. Hou, J. Xu, M. Di Renzo, and N. Al-Dhahir, "Reconfigurable Intelligent Surfaces: Principles and Opportunities," *IEEE Communications Surveys & Tutorials*, vol. 23, no. 3, pp. 1546–1577, 2021.
- [4] P. Mursia, S. Phang, V. Sciancalepore, G. Gradoni, and M. D. Renzo, "Sariz: Scattering aware reconfigurable intelligent surface model and optimization for complex propagation channels," *IEEE Wireless Communications Letters*, 2023.
- [5] A. Albanese, F. Devoti, V. Sciancalepore, M. Di Renzo, and X. Costa-Pérez, "MARISA: A Self-configuring Metasurfaces Absorption and Reflection Solution Towards 6G," in *IEEE INFOCOM 2022 - IEEE Conference on Computer Communications*, 2022.
- [6] J. Ye, A. Kammoun, and M.-S. Alouini, "Reconfigurable intelligent surface enabled interference nulling and signal power maximization in mmwave bands," *IEEE Transactions on Wireless Communications*, vol. 21, no. 11, pp. 9096–9113, 2022.
- [7] Z. Ma, Y. Wu, M. Xiao, G. Liu, and Z. Zhang, "Interference Suppression for Railway Wireless Communication Systems: A Reconfigurable Intelligent Surface Approach," *IEEE Transactions on Vehicular Technology*, vol. 70, pp. 11 593–11 603, 2021.
- [8] T. Hester, M. Vecerik, O. Pietquin, M. Lanctot, T. Schaul, B. Piot, D. Horgan, J. Quan, A. Sendonaris, I. Osband *et al.*, "Deep q-learning from demonstrations," in *Proceedings of the AAAI Conference on Artificial Intelligence*, vol. 32, no. 1, 2018.
- [9] A. Albanese, V. Sciancalepore, A. Banchs, and X. Costa-Perez, "LOKO: Localization-aware Roll-out Planning for Future Mobile Networks," *IEEE Transactions on Mobile Computing*, 2022.
- [10] R. Brem and T. F. Eibert, "A Shooting and Bouncing Ray (SBR) Modeling Framework Involving Dielectrics and Perfect Conductors," *IEEE Transactions on Antennas and Propagation*, vol. 63, no. 8, pp. 3599–3609, 2015.
- [11] H. Lu, Y. Zeng, S. Jin, and R. Zhang, "Aerial Intelligent Reflecting Surface: Joint Placement and Passive Beamforming Design With 3D Beam Flattening," *IEEE Transactions on Wireless Communications*, vol. 20, no. 7, pp. 4128–4143, 2021.
- [12] B. Di, H. Zhang, L. Song, Y. Li, Z. Han, and H. V. Poor, "Hybrid beamforming for reconfigurable intelligent surface based multi-user communications: Achievable rates with limited discrete phase shifts," *IEEE Journal on Selected Areas in Communications*, vol. 38, no. 8, pp. 1809–1822, 2020.
- [13] A. Albanese, G. Encinas Lago, V. Sciancalepore, X. Costa-Pérez, D.-T. Phan-Huy, and R. Stéphane, "RIS-Aware Indoor Network Planning: The Rennes Railway Station Case," in *IEEE ICC 2022 - IEEE International Conference on Communications*, 2022.
- [14] M. Rossanese, P. Mursia, A. Garcia-Saavedra, V. Sciancalepore, A. Asadi, and X. Costa-Perez, "Designing, building, and characterizing rf switch-based reconfigurable intelligent surfaces," in *Proceedings of the 16th ACM Workshop on Wireless Network Testbeds, Experimental evaluation & Characterization*, 2022, pp. 69–76.
- [15] R. Flamini, D. De Donno, J. Gambini, F. Giuppi, C. Mazzucco, A. Milani, and L. Resteghini, "Toward a heterogeneous smart electromagnetic environment for millimeter-wave communications: An industrial viewpoint," *IEEE Transactions on Antennas and Propagation*, vol. 70, no. 10, pp. 8898–8910, 2022.
- [16] P. Series, "Effects of building materials and structures on radiowave propagation above about 100 MHz," *Recommendation ITU-R*, 2015.
- [17] "Adam: A method for stochastic optimization, author=Kingma, Diederik P and Ba, Jimmy," *ICLR*, 2015.
- [18] E. Amaldi, A. Capone, and F. Malucelli, "Planning UMTS base station location: optimization models with power control and algorithms," *IEEE Transactions on Wireless Communications*, no. 5, pp. 939–952, 2003.
- [19] J. G. Andrews, F. Baccelli, and R. K. Ganti, "A Tractable Approach to Coverage and Rate in Cellular Networks," *IEEE Transactions on Communications*, vol. 59, no. 11, pp. 3122–3134, 2011.
- [20] E. Moro, I. Filippini, A. Capone, and D. De Donno, "Planning Mm-Wave Access Networks With Reconfigurable Intelligent Surfaces," in *2021 IEEE 32nd Annual International Symposium on Personal, Indoor and Mobile Radio Communications (PIMRC)*, 2021, pp. 1401–1407.
- [21] Z. Xiong, Y. Zhang, D. Niyato, R. Deng, P. Wang, and L.-C. Wang, "Deep reinforcement learning for mobile 5G and beyond: Fundamentals, applications, and challenges," *IEEE Vehicular Technology Magazine*, vol. 14, no. 2, pp. 44–52, 2019.
- [22] J. Kaur, M. A. Khan, M. Iftikhar, M. Imran, and Q. E. U. Haq, "Machine learning techniques for 5G and beyond," *IEEE Access*, vol. 9, pp. 23 472–23 488, 2021.
- [23] X. Lin, M. Chen, H. Rydén, J. Jeong, H. Lee, M. Sundberg, R. Timo, H. S. Razaghi, and H. V. Poor, "Fueling the Next Quantum Leap in Cellular Networks: Embracing AI in 5G Evolution towards 6G," *arXiv preprint arXiv:2111.10663*, 2021.
- [24] Z. Yang, Y. Liu, Y. Chen, and N. Al-Dhahir, "Machine Learning for User Partitioning and Phase Shifters Design in RIS-Aided NOMA Networks," *IEEE Transactions on Communications*, vol. 69, pp. 7414–7428, 2021.
- [25] Y. Zhang, M. Alrabeiah, and A. Alkhateeb, "Reinforcement learning of beam codebooks in millimeter wave and terahertz MIMO systems," *IEEE Transactions on Communications*, vol. 70, no. 2, pp. 904–919, 2021.
- [26] J. Ye and Y.-J. A. Zhang, "DRAG: Deep Reinforcement Learning Based Base Station Activation in Heterogeneous Networks," *IEEE Transactions on Mobile Computing*, vol. 19, no. 9, pp. 2076–2087, 2020.
- [27] G. B. Tarekegn, R.-T. Juang, H.-P. Lin, Y. Y. Munaye, L.-C. Wang, and M. A. Bitew, "Deep-Reinforcement-Learning-Based Drone Base Station Deployment for Wireless Communication Services," *IEEE Internet of Things Journal*, vol. 9, no. 21, pp. 21 899–21 915, 2022.
- [28] S.-Y. Lien and D.-J. Deng, "Autonomous Non-Terrestrial Base Station Deployment for Non-Terrestrial Networks: A Reinforcement Learning Approach," *IEEE Transactions on Vehicular Technology*, 2022.

- [29] M. Botvinick, S. Ritter, J. X. Wang, Z. Kurth-Nelson, C. Blundell, and D. Hassabis, "Reinforcement learning, fast and slow," *Trends in cognitive sciences*, vol. 23, no. 5, pp. 408–422, 2019.
- [30] Y. Fenjira and H. Benbrahim, "Deep Reinforcement Learning Overview of the state of the Art." *Journal of Automation, Mobile Robotics and Intelligent Systems*, pp. 20–39, 2018.